Christoph Kern
Andreas Jess*

On the Role of Radial Dispersion in the Behavior of a Cooled Fixed-Bed Reactor: Numerical Investigation of Fischer–Tropsch Synthesis with a Cobalt-Based Catalyst

The impact of radial dispersion of both heat and mass on the behavior of cooled fixed-bed reactors was explored using a two-dimensional reactor model. This study accounted for dispersion through an effective radial thermal conductivity (λ_{rad}) and a radial dispersion coefficient of mass (D_{rad}), with Fischer–Tropsch synthesis serving as an illustrative process example. Under moderate reaction conditions and hence still rather gentle radial temperature profiles, the effect of mass dispersion on reactor performance was found to be minimal, even if disregarded ($D_{rad} = 0$), whereas dispersion of heat (λ_{rad}) always significantly impacts reactor behavior. Nevertheless, for precise thermal runaway predictions by a reactor model, incorporating mass dispersion by a realistic D_{rad} value is essential.

Keywords: Fischer–Tropsch synthesis, Fixed-bed, Radial dispersion of mass and heat

Received: April 22, 2024; *accepted:* July 18, 2024

DOI: 10.1002/ceat.202400201

Supporting Information available online

1 Introduction

Multitubular reactors are frequently used for highly exothermic reactions, such as the oxidation of naphthalene or *o*-xylene to phthalic anhydride (PA), production of synthetic natural gas via methanation, methanol synthesis, or Fischer–Tropsch synthesis (FTS). These fixed-bed reactors cool individual tubes, numbering in the thousands and typically measuring 2–6 cm in diameter, by circulating boiling water around them or, for processes requiring cooling temperatures above approximately 350 °C like PA production, by using molten salt.

A critical issue with these reactors is the risk of temperature runaway, making it essential to analyze their behavior by computer simulations based on a reliable mathematical model, which precisely forecasts temperature and concentration profiles across various design and operational parameters, including tube diameter and length, cooling temperature, and fluid velocity. Two-dimensional (2D) models, which consider the radial transport of heat and occasionally of mass, are commonly utilized to address axial and radial temperature gradients within the fixed bed. This 2D approach is advised for a thorough examination of the reactor behavior, particularly for accurately predicting runaway, in contrast to one-dimensional models, where heat transport resistances are lumped at the tube wall [1–5].

In recent studies, we introduced a sophisticated 2D model for a cooled FTS fixed-bed reactor using a cobalt catalyst [6–9]. It was, therefore, logical to apply this model to specifically investigate now also the impact of radial transport of mass and to a certain extent also of heat in reactor modeling.

Intense cooling by boiling water creates distinct radial temperature profiles in the bed, which, in turn, significantly affects the reaction rate: Under the conditions of this study, a cooling temperature of 214 °C and a peak value of 240 °C in the tube center are typical, with the rate in the center then being about twice that near the wall.

While the effect of radial heat dispersion is well-documented, the impact of radial mass dispersion on reactor dynamics is less understood. For FTS and other technically significant reactions mentioned above, the role of molecular diffusion in radial dispersion is negligible. Radial dispersion of mass (and similarly of heat) in the FTS reactor primarily results from longitudinal stream splitting and sidestepping among particles (eddy dispersion). One key distinction between radial dispersion of mass and heat in a cooled fixed-bed reactor is that eddy dispersion always tends to even out radial concentrations and to a much lesser extent radial temperature profiles. As a consequence, intensely cooled fixed beds maintain sharp axial and radial temperature profiles, whereas, for mass, the wall naturally acts as a barrier, resulting in much less pronounced radial concentration profiles.

This study aims to address and answer, at least for FTS, the following four questions:

Christoph Kern, Andreas Jess (jess@uni-bayreuth.de)
Chair of Chemical Engineering, Centre of Energy Technology, University of Bayreuth, Universitätsstraße 30, 95440, Bayreuth, Germany.

1. To what extent do radial gradients of concentration (specifically reactant CO) form?
2. Does a radial concentration gradient (c_{CO}) significantly affect reactor behavior, including temperature profiles and achieved conversion, although despite contrary claims by Carberry based on a 2D model simulation of naphthalene oxidation to PA [10]?
3. Has a radial gradient of c_{CO} an influence on the reactor's thermal sensitivity (risk of runaway)?
4. What are the differences between a reactor model assuming as limits plug flow (no radial c_{CO} gradient) or no radial dispersion of mass (maximum gradient), or using a realistic value of the radial dispersion coefficient of mass based on established literature correlations [5, 10–21]?

This paper only briefly discusses general aspects of FTS, intrinsic/effective kinetics of a cobalt catalyst, and characteristics of the utilized 2D model, with detailed information available in previously published works [6–9], including rate equations and mass/heat transfer correlations beyond radial dispersion, outlined in Sect. 2.3.

2 Methodology: Kinetics of FTS and Multitubular FTS Reactor Model

2.1 Intrinsic and Effective Reaction Kinetics of FTS

FTS is an option to produce liquid fuels like diesel or jet fuel from sources other than crude oil. Currently, syngas for FTS, comprising CO and H_2, is primarily derived from coal or natural gas. However, future prospects may include nonfossil sources and renewable electricity: H_2 could be produced through water electrolysis powered by solar and wind energy, while CO_2 might be captured from the flue gases of power plants or the off-gases of industries like steel, cement, or chemicals. Concentrated CO_2 could then serve as a carbon source for syngas, converted to CO via the reverse water–gas shift reaction or potentially through the co-electrolysis of CO_2 and H_2O.

The primary reaction of FTS, leading predominantly to paraffinic C_{2+}-hydrocarbons, is as follows:

$$\mathrm{CO} + 2\mathrm{H_2} \rightarrow (-\mathrm{CH_2}-) + \mathrm{H_2O} \quad \Delta_R H^0_{\mathrm{CH_2}298} = -152\ \mathrm{KJ\ mol^{-1}} \tag{1}$$

For a reliable kinetic description of FTS, methane formation should be treated separately:

$$\mathrm{CO} + 3\mathrm{H_2} \rightarrow \mathrm{CH_4} + \mathrm{H_2O} \quad \Delta_R H^0_{\mathrm{CH_4}298} = -206\ \mathrm{kJ\ mol^{-1}}. \tag{2}$$

The intrinsic rates for methane ($r_{m,\mathrm{CO,CH_4}}$) and C_{2+}-hydrocarbons ($r_{m,\mathrm{CO,C_{2+}}}$), along with internal diffusion limitations, have been experimentally determined in prior studies for a Pt promoted (0.03 wt% Pt for Co reduction) 10 wt% Co/γ-Al_2O_3 catalyst [6, 22–26]. Both rates adhere to Langmuir–Hinshelwood kinetics, accounting for the influences of CO and H_2 concentrations [6, 22–28]. The total intrinsic rate combines these rates, as CO_2 formation via water–gas shift is minimal for Co catalysts:

$$r_{m,\mathrm{CO}} = \frac{d\dot{n}_{\mathrm{CO}}}{dm_{\mathrm{cat}}} = C_a(r_{m,\mathrm{CO,CH_4}} + r_{m,\mathrm{CO,C_{2+}}}). \tag{3}$$

In Eq. (3), the activity coefficient C_a reflects the Co content and intrinsic activity, with the baseline of one for 10 % Co. Increasing the Co content enhances C_a. FTS catalysts typically contain up to 30 wt% Co ($C_a \approx 3$), and this value is assumed throughout this study.

A steam inhibition is also considered, and our experiments indicate [8]:

$$r_{m,\mathrm{CO,H_2O}} = r_{m,\mathrm{CO}}\left(1 - \frac{c_{\mathrm{H_2O}}}{472\ \mathrm{mol\ m^{-3}}}\right). \tag{4}$$

A value of $c_{\mathrm{H_2O}}$ of 120 mol m^{-3}, corresponding to a CO conversion of 60 %, reduces the rate by 25 %.

Eqs. (3) and (4) reflect only the intrinsic rate, but pore diffusion limitations lead to a reduced effective rate for millimeter-sized particles to mitigate excessive pressure drop. The effective rate, incorporating the pore effectiveness factor η_{pore} (details to calculate η_{pore} are given in [6–9]) is

$$r_{m,\mathrm{CO,eff}} = \eta_{\mathrm{pore}} r_{m,\mathrm{CO,H_2O}}, \tag{5}$$

where η_{pore} is significantly affected by temperature. For the particle diameter d_p of 3 mm assumed here, η_{pore} is below one above 180 °C, dropping to 0.2 for 240 °C [6–8]. This leads to a higher molar H_2-to-CO ratio in the particles relative to the bulk phase, typically two, enhancing undesired CH_4 formation over C_{2+}-HCs as the diffusion coefficient of H_2 in liquid HCs is double that of CO. This effect intensifies above 240 °C, with CH_4 selectivity surpassing 20 % versus 10 % in the absence of diffusion limitations. Additionally, we investigated peak temperature values (T_{max}) exceeding 240 °C to assess the reactor's thermal sensitivity (risk of runaway), simplistically maintaining that $S_{\mathrm{CH_4}}$ is 20 %. The stoichiometric H_2-to-CO ratio thus becomes 2.2, per the aforementioned reactions, ensuring (for simplification) always identical H_2 and CO conversions for the feed gas used in this study.

2.2 2D Model of Cooled Multitubular Fixed-Bed FTS Reactor

Eqs. (6) and (7) represent the mass and heat balance for a differential tube section (dz), where R1 denotes the reaction of CO to CH_4 and R2 represents the reaction to C_{2+}-hydrocarbons:

$$\frac{d\,(c_i\,u_s)}{dz} = \varepsilon_{\mathrm{bed}}\ D_{\mathrm{rad}}\left(\frac{1}{r}\frac{dT}{dr} + \frac{d^2T}{dr^2}\right) + \left(r_{m,\mathrm{CO,R1,eff}} + r_{m,\mathrm{CO,R2,eff}}\right)\rho_{\mathrm{bed}}, \tag{6}$$

$$c_p\,c_g\,\frac{d\,(T\,u_s)}{dz} = \lambda_{\mathrm{rad}}\left(\frac{1}{r}\frac{dT}{dr} + \frac{d^2T}{dr^2}\right) + \left(r_{m,\mathrm{CO,R1,\ eff}}\,(-\Delta_R H_{\mathrm{R1}}) + r_{m,\mathrm{CO,R2,eff}}\,(-\Delta_R H_{\mathrm{R2}})\right)\rho_{\mathrm{bed}}. \tag{7}$$

In addition to intrinsic and effective kinetics, the model incorporates several critical aspects.

The heat released by FTS dissipates through the pseudo-homogeneous phase (consisting of both catalyst and gas) within the reactor bed to the tube wall by radial dispersion of heat. It then transfers through the tube wall and ultimately to the cooling fluid, which is boiling water. Considering the adiabatic

temperature increase due to the FTS reaction can reach 1000 K for complete CO conversion, while the permissible increase to prevent thermal runaway is below 30 K [6, 8], effective cooling becomes imperative. This need is addressed by employing small tubes, in this study with a diameter of 3 cm. The radial dispersion/conduction of heat in the bed up to the inner tube wall is determined by the effective thermal conductivity λ_{rad} (see Sect. 2.3). At the inner tube wall, the heat transfer coefficient $\alpha_{w,\,int}$ comes into play, accounting for the thermal resistance at the inner wall, a result of the bed's high porosity near the wall. This scenario implies a temperature discontinuity ("jump") at the wall. Heat conduction through the wall, a minor contributor to the overall thermal resistance, and the external heat transfer from the tube's outer surface to the boiling water ($\alpha_{w,ex}$) are included. All heat transfer parameters are calculated by literature correlations, as outlined in [8, 9].

Table 1. Main results of reactor modeling of the base case of $T_{cool} = 213.8$ °C.

Conversion of CO X_{CO} ($= X_{H_2}$)	65.4%
Maximum axial temperature T_{max} (at $r = 0$) reached at $z = 1.9$ m	240.0 °C
Pore effectiveness factor η_{pore} (at T_{max}, $z = 1.9$ m, $r = 0$)	0.19
Radial dispersion parameter/coefficient $\varepsilon_{bed} D_{rad}$	1.5×10^{-4} m^2 s^{-1}
Effective radial thermal conductivity λ_{rad} (at T_{max}, $z = 1.9$ m)	4.4 W m^{-1} K^{-1}
Internal heat transfer coefficient (bed to internal tube wall) $\alpha_{w,\,int}$ ($z = 1.9$ m)	1007 W m^{-2} K^{-1}
External heat transfer coefficient (external wall to boiling water) $\alpha_{w,ex}$ ($z = 1.9$ m)	1370 W m^{-2} K^{-1}
Radial heat flux (wall to boiling water) $\dot{q}$ (at T_{max}, $z = 1.9$ m)	5300 W m^{-2}
Pressure drop Δp_{bed}	1.18 bar

The model also incorporates changes in the molar flow rate due to the FTS reaction and the pressure drop, computed via the Ergun equation [27]. Both aspects influence the superficial gas velocity and, consequently, the residence time and the reactor behavior regarding temperature and conversion.

Radial dispersion of mass is taken into account, with further details provided in Sect. 2.3.

Axial dispersion of mass and heat is not considered relevant for this model, as it affects scenarios with much steeper axial gradients of concentration or temperature over a length spanning only a few particles [9]. For the numerical analysis, the differential equations (DEs) of the mass and heat balance were solved by *Presto Kinetics*, a reliable solver of DEs (CiT GmbH, Rastede, Germany).

2.3 Radial Dispersion of Mass and Heat in the FTS Reactor

The effective radial thermal conductivity in a fixed bed can be calculated using a correlation incorporating the Reynolds and the Prandtl number ($Re_p = u_s d_p/\nu_g$; $Pr = \nu_g \rho_g c_p/\lambda_g$) [11, 12]:

$$\lambda_{rad} = 4\lambda_g + \frac{Re_p Pr}{7\left[2 - \left(1 - 2\,\frac{d_p}{d_{t,int}}\right)^2\right]}\lambda_g. \tag{8a}$$

The prefactor 4 in the first term of Eq. (8a), indicative of the static contribution without gas flow ($\lambda_{rad} = 4\lambda_g$ for $Re_p = 0$), depends on the thermal conductivity ratio of particle to fluid and ranges from 1.5 for a ratio of 2 to approximately 4 for a value > 10 [11]. Nonetheless, the significance of the exact value of the prefactor is minimal for Re_p typically encountered in fixed-bed processes (see below).

For the FTS reactor examined in this study, with a d_p-to-$d_{t,\,int}$ ratio of 0.1, λ_{rad} simplifies to

$$\lambda_{rad} = 4\lambda_g + \frac{u_s d_p \rho_g c_p}{9.5}. \tag{8b}$$

Similarly, the radial dispersion coefficient of mass, D_{rad}, is determined with the Schmidt number ($Sc = \nu_g/D_{CO,mol}$) and a bed tortuosity (τ_{bed}) of approximately 1.5 [5, 10–21] by

$$\varepsilon_{bed} D_{rad} = \frac{\varepsilon_{bed}}{\tau_{bed}} D_{CO,mol} + \frac{Re_p\, Sc}{10} D_{CO,mol} \tag{9a}$$

$$\varepsilon_{bed} D_{rad} = 0.3 D_{CO,mol} + \frac{u_s d_p}{10}. \tag{9b}$$

This tortuosity takes into account that the void space in the bed does not provide straight-line paths, thereby extending the dispersion path on average by 50 % [15, 20]:

In the context of FTS, and likely for fixed-bed processes in general, eddy dispersion—the second term in Eqs. (8b) and (9b)—dominate $\varepsilon_{bed} D_{rad}$ and λ_{rad}. In this work, with Re_p of 650, Pr of 0.5, and Sc of 0.35, the static contributions, $4\lambda_g$, and $0.3 D_{mol,\,CO}$, are almost negligible, accounting for only 10 % of λ_{rad} and even 1 % of $\varepsilon_{bed} D_{rad}$ (see values listed in Tab. 1).

Radial dispersion in a fixed bed is often also elucidated through radial Peclet numbers, $Pe_{h,\,rad} = u_s d_p \rho_g c_p \lambda_{rad}^{-1} = Re_p Sc \lambda_g \lambda_{rad}^{-1}$ for heat and $Pe_{m,\,rad} = u_s d_p\ (\varepsilon_{bed} D_{rad})^{-1} = Re_p Pr D_{CO,\,mol}\ (\varepsilon_{bed} D_{rad})^{-1}$ for mass. The formulation of $Pe_{h,\,rad}$ employs the superficial fluid velocity (u_s) instead of the interstitial (u_s/ε_{bed}) used in $Pe_{m,\,rad}$. This distinction arises as heat conduction, encapsulating both gas and solid phase contributions, is not confined to the bed's void space, unlike mass dispersion. Experience suggests a value of about 10 for both Peclet numbers when $Re_p > 100$ [10–21], leading to $\lambda_{rad} \approx 0.1\, u_s d_p \rho_g c_p$ and $\varepsilon_{bed} D_{rad} \approx 0.1\, u_s d_p$. Consequently, radial dispersion of mass and heat are then interrelated, with $\varepsilon_{bed} D_{rad}$ roughly equating $\lambda_{rad}\,(\rho_g c_p)^{-1}$. Under the conditions for FTS in this study, the actual Peclet numbers are 8.5 for $Pe_{h,\,rad}$ and 9.9 for $Pe_{m,\,rad}$, closely approaching the thresholds of 9.5 (see Eq. (8b) for $\lambda_{rad} \gg \lambda_g$) and 10 (see Eq. (9b) for $D_{rad} \gg D_{CO,\,mol}$.

3 Simulation of Multitubular FTS Reactor for Different Degrees of Radial Dispersion of Mass

Fig. 1 illustrates the impact of the cooling temperature, T_{cool}, on the axial temperature profile for two distinct scenarios of radial dispersion coefficients, a realistic value of 1.5×10^{-4} m^2 s^{-1} for

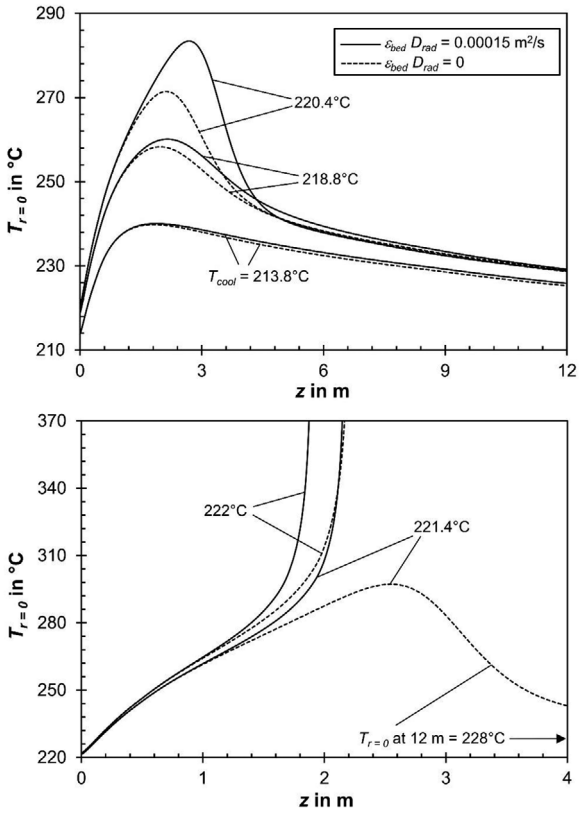

Figure 1. Influence of T_{cool} on axial temperature profiles for a realistic radial mass dispersion, that is, $\varepsilon_{bed}D_{rad} = 1.5 \times 10^{-4}$ m^2 s^{-1} according to Eq. (9b), and no dispersion ($D_{rad} = 0$). The corresponding profiles of X_{CO} are depicted in Fig. S1 (in the supporting information [SI]).

$\varepsilon_{bed}D_{rad}$ as determined by Eq. (9b), and a scenario representing the limit of no radial mixing ($D_{rad} = 0$).

Fig. 2 presents radial temperature profiles at a rather low (standard case) and a high cooling temperature for $\varepsilon_{bed}D_{rad} = 1.5 \times 10^{-4}$ m^2 s^{-1} and for $D_{rad} = 0$. In each case, the profiles are depicted at the axial location of the axial peak temperature. In the first (realistic) scenario, the target peak temperature of 240 °C is precisely met for T_{cool} of 213.8 °C (base case). In the second scenario ($D_{rad} = 0$), this peak value is only negligibly lower (239.8 °C). But in the case of a higher T_{cool} of 220.4 °C, which already approaches the threshold of temperature runaway, the peak temperatures and the radial temperature profiles differ from each other, and higher temperatures are reached, if a realistic degree of radial dispersion of mass is considered in the reactor simulation.

Principal other outcomes of the simulation for the realistic value of $\varepsilon_{bed}D_{rad}$ of 1.5×10^{-4} m^2 s^{-1} and a peak temperature of 240 °C are summarized in Tab. 1; operational conditions and data of chemical media are listed in Tab. 2. Additionally, Tab. 3 catalogs the CO conversion reached at the axial position of the peak temperature (z_{max}) and the tube's end ($z = 12$ m) for different values of T_{cool}, along with the (relative) radial deviation of c_{CO} at z_{max}. These metrics are also reported for $D_{rad} = 0$ and for a scenario emulating plug flow by setting $\varepsilon_{bed}D_{rad}$ to an extremely high value of 1 m^2 s^{-1}, by far never reached in FTS

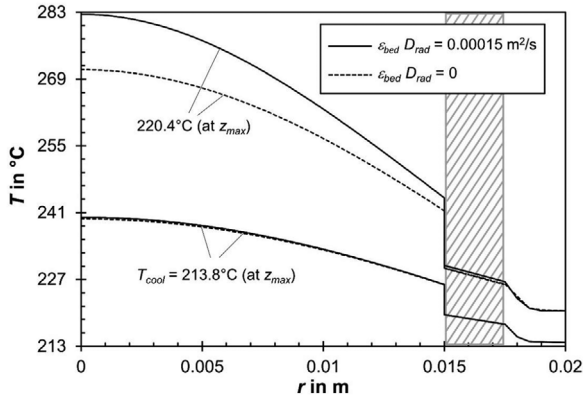

Figure 2. Radial temperature profiles for two values of T_{cool} for $\varepsilon_{bed}D_{rad} = 1.5 \times 10^{-4}$ m^2 s^{-1} or 0. The profiles are given at z_{max}, where the axial peak temperature is just reached (Fig. 1). Profiles from the external wall into the boiling water ($r > 0.0175$ m) are only schematically shown.

(Re_p would then have to be 6700 times higher, 4×10^6 instead of here 650!).

Fig. 3 examines the influence of $\varepsilon_{bed}D_{rad}$ on the CO conversion for a high value of T_{cool} (220.4 °C), both at the point of the maximum axial peak temperature (left) and at the reactor outlet (right).

The conclusions based on Figs. 1–3 are unequivocal: Under moderate reaction conditions, here specifically for T_{cool} below 219°C, the impact of radial mass dispersion is virtually inconsequential. Whether $\varepsilon_{bed}D_{rad}$ is set to zero, to a realistic value of 1.5×10^{-4} m^2 s^{-1} or to 1 m^2 s^{-1} (emulating plug flow), it bears

Table 2. Operational conditions (for $T_{max} = 240$ °C) and data on chemical media (230 °C, 30 bar).

Length of reactor (single tube) L_t	12 m
Internal tube diameter $d_{t,\,int}$ (thickness of tube wall s_{wall})	3 cm (5 mm)
Initial content of CO, H_2, and CH_4[a]	20 %, 44 %, and 36 %
Cooling temperature T_{cool} (= inlet temperature)	213.8 °C
Initial superficial gas velocity $u_{s,\,z=0}$	0.5 m s^{-1}
Total pressure p (reactor inlet)	30 bar
Diameter of spherical catalyst particles d_p	3 mm
Bulk density of bed/catalyst ρ_{bed}	960 kg m^{-3}
Porosity of fixed bed ε_{bed}	0.4
Heat capacity of gas mixture c_p	35 J mol^{-1} K^{-1}
Density of gas mixture ρ_g	730 mol m^{-3}
Thermal conductivity of gas mixture λ_g	0.12 W m^{-1} K^{-1}
Kinematic viscosity of gas mixture ν_g	2.3×10^{-6} m^2 s^{-1}
Thermal conductivity of wall material (steel) λ_{wall}	15 m^{-1} K^{-1}

a) Typical CH_4 content related to gas recycling after separation of higher HCs and water [7–9].

Table 3. Influence of T_{cool} on reactor behavior: $X_{CO,T_{max}}$ at T_{max} reached at z_{max}, (rel.) radial deviation of c_{CO} at T_{max}, and $X_{CO,12\,m}$ at the outlet, if radial mass dispersion is neglected ($D_{rad} = 0$), for a realistic value ($\varepsilon_{bed}D_{rad} = 1.5 \times 10^{-4}$ m^2 s^{-1}), or if plug flow is assumed ($\varepsilon_{bed}D_{rad} = 1$ m^2 s^{-1}).

T_{cool} [°C]	$\varepsilon_{bed}D_{rad}$ [m^2 s^{-1}]	$X_{CO,T_{max}}$	z_{max} at T_{max} [m]	T_{max} [°C]	$\Delta c_{CO,radial}/c_{CO,r=r_{tube}}$ at z_{max}	$X_{CO,12\,m}$
213.8	0	13.4 %	1.80	239.8	6 %	64.9 %
	1.5×10^{-4}	13.9 %	1.86	240.0	0.2 %	65.4 %
	1 (plug flow)[a]	13.9 %	1.86	240.0	3×10^{-5} %	65.4 %
218.8	0	21.0 %	1.97	258.7	14 %	75.9 %
	1.5×10^{-4}	23.3 %	2.14	260.6	0.6 %	77.1 %
	1 (plug flow)[a]	23.6 %	2.14	260.8	1×10^{-4} %	77.2%
220.4	0	27.6 %	2.15	271.4	24 %	79.7 %
	1.5×10^{-4}	37.8 %	2.64	283.3	1.6 %	82.7 %
	1 (plug flow)[a]	39.9 %	2.72	285.7	2×10^{-4} %	83.1 %
221.4	0	42.0 %	2.57	297.2	51 %	83.9 %
	1.5×10^{-4} or 1	Thermal runaway				

a) A high value of ε_{bed} D_{rad} of 1 emulates plug flow as the radial c_{CO} deviation is only 2×10^{-4} %.

minimal influence on the outcomes of the simulation (T_{max}, X_{CO}), as evidenced in Tab. 3 and Figs. 1 and 2 ($T_{cool} \leq 219$ °C), and the radial deviation of c_{CO} remains under 15%. However, as conditions approach the threshold of runaway for T_{cool} above 220 °C, the deviations between radial and axial temperatures and CO conversion escalate significantly (Tab. 3 and Figs. 1–3).

Fig. 4 shows the impact of $\varepsilon_{bed}D_{rad}$ on the ignition temperature (T_{ig}) related to runaway. When dispersion is ignored ($\varepsilon_{bed}D_{rad} = 0$), T_{ig} is found to be 1 K higher compared to the realistic $\varepsilon_{bed}D_{rad}$ of 1.5×10^{-4} m^2 s^{-1}, outlined by Eq. (9b). This effect results from the then unrealistic high depletion of c_{CO} in the tube's hotter and thus critical core region, for example, for $T_{cool} =$ 221.4 °C (Fig. 5 left).

The assumption of an unrealistically high value of $\varepsilon_{bed}D_{rad}$ of, for example, 1 m^2 s^{-1} does not yield a difference in T_{ig} compared to the realistic, much lower value of 1.5×10^{-4} m^2 s^{-1}. This shows that the precise knowledge of $\varepsilon_{bed}D_{rad}$ is uncritical in simulation even to predict runaway, but ignoring radial mass dispersion results in an overrated T_{ig}, here by 1 K, underrating the danger of runaway. Consequently, the achievable CO conversion is overrated, here by two percentage points for ΔT_{cool} of 1 K, if the allowable T_{cool} is set by a certain margin below T_{ig} (e.g., by 5 K) to ensure a safe distance to runaway.

Contrastingly, the scenario changes when considering radial heat dispersion. Here, the value of λ_{rad} always significantly influences temperature profiles, conversion, and runaway behavior. For instance, conducting a simulation for $T_{cool} =$ 213.8 °C with λ_{rad} 20 % lower than derived by Eq. (8b) leads to a CO conversion of 69 % compared to realistically 65 %, resulting from the overrated peak temperature of 250 °C compared to realistically 240 °C, both computed with $\varepsilon_{bed}D_{rad} = 1.5 \times 10^{-4}$ m^2 s^{-1}. T_{ig} is then 216.5 °C, diverging from the true 220.4 °C by 4 K. A decrease of T_{cool} by this value, if needed to keep a certain safe distance to runaway, leads to a high relative decline of X_{CO} by 15 %.

A further comparison also illustrates the major influence of the accuracy of λ_{rad} on the simulation: A reduction of the value by 20 % compared to "reality" reduces T_{cool} to reach a certain target peak temperature. For 240 °C as target, T_{cool} must be already reduced to 211.3 °C compared to the real value of 213.8 °C, and X_{CO} drops from 65.4 % to 62.7 %. Note that for these reaction conditions, the same reduction of the mass dispersion term $\varepsilon_{bed}D_{rad}$ changes X_{CO} only in the third decimal of the percentage.

Fig. 5 explores the scenario of a hypothetical absence of any radial dispersion of mass ($\varepsilon_{bed}D_{rad} = 0$) on radial c_{CO} profiles for varying cooling temperatures. It highlights that significant radial gradients only emerge at relatively high temperatures, nearing runaway conditions.

The effects of the dispersion term $\varepsilon_{bed}D_{rad}$ on radial concentration profiles at the axial location of the temperature peak are illustrated in Fig. 6 and detailed in Tab. 4, using

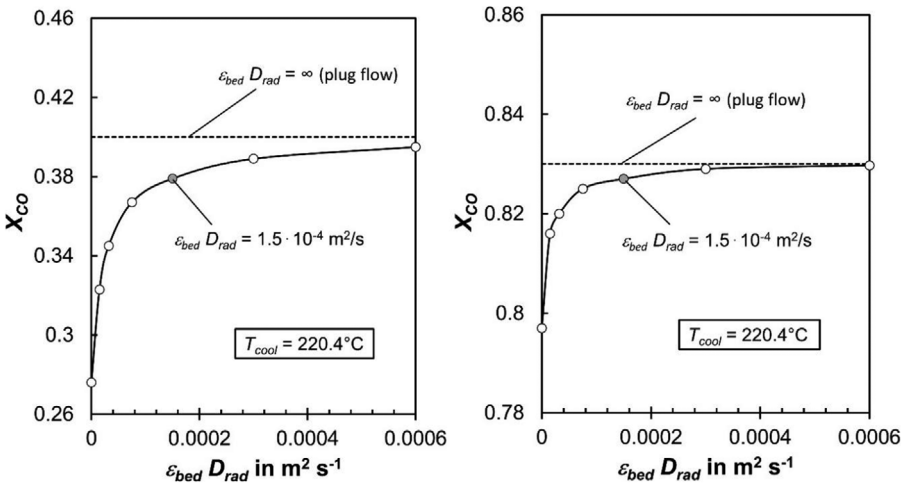

Figure 3. Influence of $\varepsilon_{bed}D_{rad}$ on X_{CO} reached at the location of T_{max} (left) and at the outlet ($z = 12$ m, right) for a rather high value of T_{cool}. For the influence of $\varepsilon_{bed}D_{rad}$ on T_{max}; see Fig. S2 (in the SI).

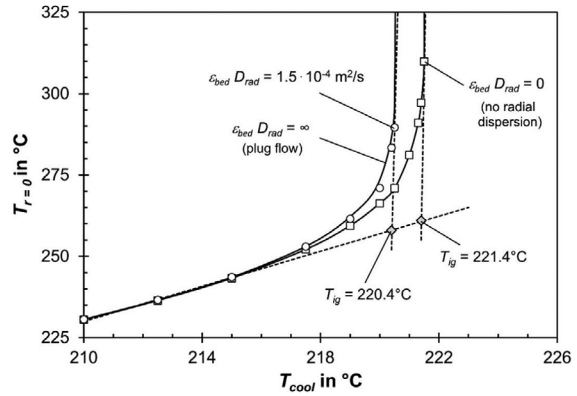

Figure 4. Influence of $\varepsilon_{bed}D_{rad}$ on maximum axial temperature in the center of the tube (r = 0) and T_{ig} (runaway), respectively, determined via tangent construction. In the base case of T_{cool} = 213.8 °C (T_{max} = 240 °C), there is a sufficient safety distance to T_{ig} of 7 K.

relative c_{CO} values against a mean located around a radial position of approximately 0.85 cm for a high T_{cool} of 220.4 °C.

In the context of Fischer–Tropsch synthesis evaluated in this study (base case), a reactor behavior closely resembling plug flow is almost achieved. This is further evidenced in Fig. 7 by the influence of Re_p on $\varepsilon_{bed}D_{rad}$, which shows that for Re_p of the simulated FTS reactor of 650, $\varepsilon_{bed}D_{rad}$ is already quite high and plug flow is almost reached. Notably, even with a tenfold reduction in $\varepsilon_{bed}D_{rad}$, the radial c_{CO} gradient remains modest with a deviation of c_{CO} of only 11 % (Fig. 6 and Tab. 4, cases 3 and 4). But when considering solely molecular diffusion and no realistic dynamic contribution to radial dispersion of mass (eddy dispersion), a pronounced radial c_{CO} profile is formed, with 24 % deviation of c_{CO}, and this profile is already close to the borderline scenario excluding any radial concentration compensation (D_{rad} = 0; 40 % deviation) (see Tab. 4, cases 1 and 2, and Fig. 6).

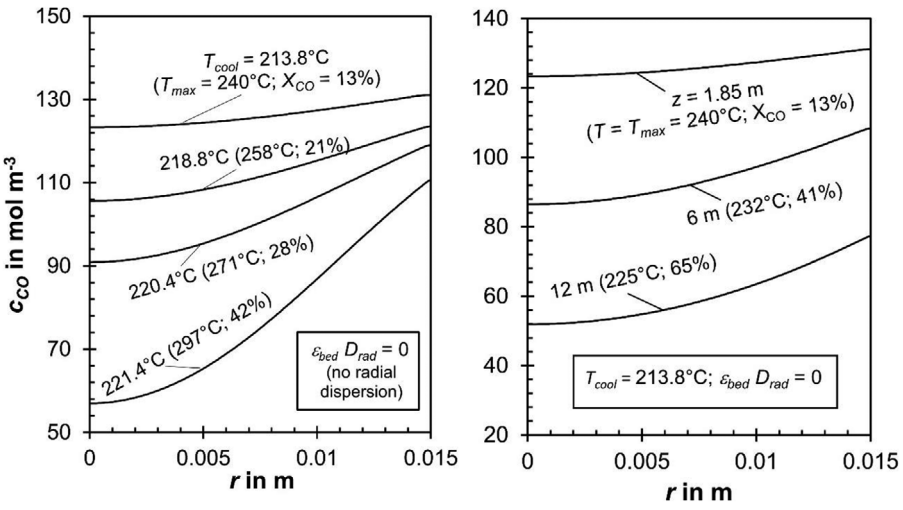

Figure 5. Modeling results for assumption (hypothetic case) of no radial dispersion ($\varepsilon_{bed}D_{rad}$ = 0): Left: Influence of T_{cool} on radial c_{CO} profiles at z_{max}, that is, the location of T_{max}; right: c_{CO} profiles at different axial positions, namely z_{max}, middle, and end of the tube, for T_{cool} = 213.8 °C.

Figs. S3–S5 (in the SI) examine an exceptional scenario, while not directly pertinent to FTS, but probably offers insights for other processes and is definitely scientifically interesting and unexpected: This scenario investigates the effects of very high temperatures exceeding 400 °C, indicative of thermal runaway conditions. Under such circumstances, minimal or no radial dispersion induces pronounced radial concentration gradients, in extreme cases characterized by a near absence of reactants (here CO and H_2) near the tube center. Interestingly, this results in the radial temperature profile peaking within the interior regions of the fixed bed rather than at its center.

Additionally, Figs. S6–S8 (in the SI) present simulations exploring the equalization of radial temperature and concentration profiles in an adiabatic fixed-bed devoid of reaction and also of cooling, situated directly downstream of an FTS reactor. Hence, pronounced radial profiles of T and c_{CO} are generated and transmitted from the outlet of the FTS reactor to the inlet of the succeeding adiabatic and unreactive packed bed. This hypothetical yet enlightening scenario demonstrates the strong basic similarities between the dispersion of mass and heat within a fixed bed under technically relevant gas velocities ($Re_p > 100$), as radial dispersion of both mass and heat homogenizes quickly and to the same extent the respective radial profiles of T and c_{CO}.

Despite these similarities, the intensive cooling required for a real fixed-bed reactor undergoing an exothermic reaction ensures the maintenance of sharp radial (and axial) temperature profiles. Conversely, pronounced radial concentration gradients are seldom observed as the tube's wall acts as a barrier for mass transport (but promotes heat transport to the cooling medium).

4 Conclusions

A comprehensive 2D numerical model was employed to simulate the behavior of a cooled multitubular fixed-bed reactor. This study particularly examines the impact of radial dispersion of mass and partly also of heat on the performance of fixed-bed reactors, using Fischer–Tropsch synthesis as a case study. Reactor simulations were compared under various assumptions, for example, plug flow conditions, indicative of perfect radial mixing without a radial gradient of CO concentration, absence of radial mass dispersion (D_{rad} = 0), resulting in maximum gradient, and a realistic D_{rad} value derived from literature correlations.

The findings show that under moderate conditions, where cooling temperatures are still sufficiently below the threshold for thermal runaway, the effect of mass dispersion is minimal. This holds true even when completely disregarded (D_{rad} = 0), with radial c_{CO}-gradients remaining small. But for accurately predicting

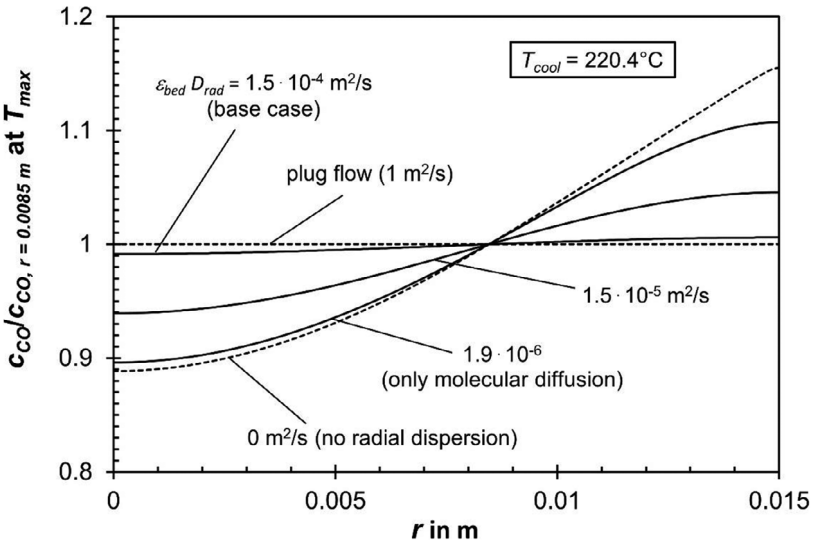

Figure 6. Influence of $\varepsilon_{bed}D_{rad}$ on radial c_{CO} profiles (relative to a mean concentration at $r = 0.85$ cm) at the axial position of T_{max}. T_{cool} is 220.4 °C, which approaches the threshold of runaway. Values regarding CO-conversion and axial peak temperatures in each case are in Tab. 4.

conditions leading to runaway, it is crucial to include a realistic value of D_{rad}.

Conversely, the dispersion of heat, namely the accuracy of the value of λ_{rad}, consistently exerts a significant influence on all aspects of reactor simulation and behavior such as temperature profiles, conversion, and parametric sensitivity (runaway).

To take stock: For a reliable simulation of a cooled fixed-bed reactor, accurate values of the parameters of radial heat transfer are an absolute must, but rough estimations of radial mass transport should also be included, at least to predict accurately the runaway behavior.

Table 4. Influence of $\varepsilon_{bed}D_{rad}$ on reactor behavior regarding CO conversion ($X_{CO,\,T_{max}}$ at T_{max} and $X_{CO,\,12\,m}$ at outlet), radial deviation of c_{CO} in the bed at T_{max} for a cooling temperature of 220.4 °C, which is just below the danger of thermal runaway; conditions in Tab. 2.

Case	$\varepsilon_{bed}D_{rad}$ [$m^2\ s^{-1}$]	$X_{CO,\,T_{max}}$ [%]	z at T_{max} [m]	T_{max} [°C]	$\Delta c_{CO,radial}/c_{CO,\,r=r_{tube}}$ [%] (see Fig. 5 left)	$X_{CO,\,12\,m}$ [%]
1	0 (no radial dispersion/diffusion)	27.2	2.13	271.0	40	79.7
2	1.9×10^{-6} (only molecular diffusion)[a]	28.1	2.18	271.7	24	80.4
3	1.5×10^{-5}	31.9	2.39	275.5	11	81.5
4	1.5×10^{-4} (base case, FTS this work)	37.8	2.64	283.3	1.6	82.7
5	2.3×10^{-4} (almost plug flow)[b]	38.9	2.65	284.1	1	82.8
6	1 (plug flow)[b]	39.9	2.72	285.7	2×10^{-4}	83.1

a) The molecular diffusion coefficient of CO ($D_{CO,\,mol}$) in H_2 (30 bar, 240 °C) is 6.5×10^{-6} $m^2\ s^{-1}$. For a stagnant bed (no gas flow), $\varepsilon_{bed}D_{rad} = \varepsilon_{bed}/\tau_{bed}D_{CO,\,mol}$ (with $\tau_{bed} \approx 1.5$), that is, the minimum of $\varepsilon_{bed}D_{rad}$ (only molecular diffusion) is 1.9×10^{-6} $m^2\ s^{-1}$, 80 times lower than realistic dispersion in the FTS reactor (case 4). b) $\varepsilon_{bed}D_{rad} = 1$ $m^2\ s^{-1}$ (case 6) equals almost perfectly plug flow (see footnote Tab. 3). For $\varepsilon_{bed}\ D_{rad} > 2.3 \times 10^{-4}$ $m^2\ s^{-1}$ (case 5), the deviation gets less than 1 %, that is, plug flow behavior is still almost reached.

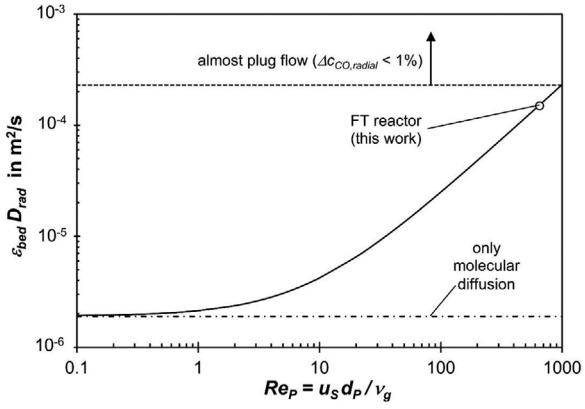

Figure 7. Influence of Re_p on radial dispersion term $\varepsilon_{bed}D_{rad}$ (FTS reactor; Eq. (9b) with $Sc = 0.7$).

Supporting Information

Supporting information for this article can be found under DOI: https://doi.org/10.1002/ceat.202400201.

Acknowledgments

Open access funding enabled and organized by Projekt DEAL.

Symbols used

C_a	[–]	coefficient of catalytic activity (= 1 for 10 wt.% Co)
c_i	[mol m^{-3}]	concentration of i (gas phase; i = CO, H_2, H_2O)

$D_{CO,mol}$	[$m^2\ s^{-1}$]	molecular diffusion coefficient of CO
m_{cat}	[kg]	mass of catalyst
$Pe_{h,rad}$	[–]	radial Peclet number of heat, $u_s d_p c_p \rho_g / \lambda_g$
$Pe_{m,rad}$	[–]	radial Peclet number of mass, $u_s\ d_p/(\varepsilon_{bed} D_{rad})$
Pr	[–]	Prandtl number, $\nu_g \rho_g c_p / \lambda_g$
r	[m]	radial distance in fixed-bed (r_t = internal radius of tube)
$r_{m,CO}$	[$mol_{CO}\ kg_{cat}^{-1}\ s^{-1}$]	intrinsic reaction rate of CO
r_{m,CO,H_2O}	[$mol_{CO}\ kg_{cat}^{-1}\ s^{-1}$]	intrinsic rate of CO, if inhibition by steam is considered
$r_{m,CO,eff}$	[$mol_{CO}\ kg_{cat}^{-1}\ s^{-1}$]	effective reaction rate of CO to methane
Re_p	[–]	Reynolds number, $u_s d_p / \nu_g$
Sc	[–]	Schmidt number, $\nu_g / D_{CO,mol}$
T	[°C, K]	Temperature
X_{CO}	[–]	conversion of CO
z	[m]	axial coordinate in fixed bed

Greek letters

$\Delta_R H_i$	[$J\ mol_{CO}^{-1}$]	enthalpy of reaction, i = reaction of CO to methane or to C_{2+}-HCs
τ_{bed}	[–]	tortuosity of bed (1.5)

Abbreviations

C_{2+}	hydrocarbons with two or more carbon atoms
(—CH_2—)	methylene group of a normal paraffin
FTS	Fischer–Tropsch synthesis
HC	hydrocarbons
PA	phthalic anhydride
SI	supporting information

References

[1] F. Sauerhöfer-Rodrigo, I. Diaz, M. Rodrigez, P. Perez, *Rev. Chem. Eng.* **2024**, *40*, 151. DOI: https://doi.org/10.1515/revce-2022-0041

[2] J. R. G. Sanchez-Lopez, A. Martinez-Hernandez, A. Hernandez-Ramitez, *Rev. Chem. Eng.* **2017**, *33* (*2*), 109. DOI: https://doi.org/10.1515/revce-2015-0044

[3] C. I. Mendez, J. Ancheyta, F. Trejo, *Energy Fuels*, **2017**, *31*, 13011. DOI: https://doi.org/10.1021/acs.energyfuels.7b01431

[4] A. Jess, P. Wasserscheid, *Chemical Technology: From Principles to Processes*, 2nd ed., Wiley, Weinheim, Germany **2020**.

[5] C. Kern, A. Jess, *Chem. Eng. Technol.* **2009**, *32* (*8*), 1164–1175. https://doi.org/10.1002/ceat.20090013

[6] C. Kern, A. Jess, *Catal. Sci. Technol.* **2023**, *13*, 2212–2222. DOI: https://doi.org/10.1039/D3CY00093A

[7] C. Kern, A. Jess, *Catal. Sci. Technol.* **2023**, *13*, 516–527. DOI: https://doi.org/10.1039/D2CY01804G

[8] J. J. Carberry, D. White, *Ind. Eng. Chem.* **1969**, *61* (*7*), 27–35. DOI: https://doi.org/10.1021/ie50715a008

[9] E.-U. Schlünder, E. Tsotsas, *Wärmeübertragung in Festbetten, durchmischten Schüttgütern und Wirbelschichten*, Georg Thieme, Stuttgart, Germany **1988**.

[10] C. Kern, A. Jess, *Processes* **2023**, *11*, 3281. DOI: https://doi.org/10.3390/pr11123281

[11] R. W. Fahien, J. M. Smith, *AIChE J.* **1955**, *1* (*1*), 28–37. DOI: https://doi.org/10.1002/aic.690010104

[12] C. Kern, A. Jess, *Energy Technol.* **2024**, 2301534. DOI: https://doi.org/10.1002/ente.202301534

[13] W. E. Ranz, *Chem. Eng. Prog.* **1952**, *48*, 247–253.

[14] A. G. Dixon, *Chem. Eng. Commun.* **1988**, *71* (*1*), 217–237. DOI: https://doi.org/10.1080/00986448808940426

[15] Verein Deutscher Ingenieure (ed.), *VDI-Wärmeatlas: Berechnungsblätter für den Wärmeübergang*, Springer, Berlin/Heidelberg, Germany **2002**.

[16] J. G. H. Borkink, K. R. Westerterp, *AIChE J.* **1992**, *38* (*5*), 641–797. DOI: https://doi.org/10.1002/aic.690380607

[17] F. Pöhlmann, A. Jess, *Energy Technol.* **2016**, *4*, 55–64. DOI: https://doi.org/10.1002/ente.201500216

[18] F. Pöhlmann, S. Rössler, C. Kern, A. Jess, *Catal. Sci. Technol.* **2016**, *6*, 6593–6604. DOI: https://doi.org/10.1039/C6CY00941G

[19] M. F. Edwards, J. F. Richardson, *Chem. Eng. Sci.* **1968**, *23* (*2*), 109–123. DOI: https://doi.org/10.1016/0009-2509(68)87056-3

[20] F. Pöhlmann, *Zusammenspiel von chemischer Reaktion und Porendiffusion bei der kobaltkatalysierten Fischer-Tropsch-Synthese unter Einsatz von CO_2-haltigem Synthesegas*, Ph.D. Thesis, University Bayreuth **2017**.

[21] G. F. Froment, *Ind. Eng. Chem.* **1967**, *59* (*2*), 18–27. DOI: https://doi.org/10.1021/ie50686a006

[22] Tsotsas, E.-U. Schlünder, *Chem. Eng. Sci.* **1988**, *43* (*5*), 1200–1203. DOI: https://doi.org/10.1016/0009-2509(88)85081-4

[23] B. D. Kulkarni, L. K. Doraiswamy, *Catal. Rev. Sci. Eng.* **1980**, *22* (*3*), 431–483. DOI: https://doi.org/10.1080/03602458008067540

[24] J. J. Carberry, *Chemical and Catalytic Reaction Engineering*, 2nd ed., Dover, Mineola, NY **2001**.

[25] F. Pöhlmann, A. Jess, *Catal. Today* **2016**, *275*, 172–182. DOI: https://doi.org/10.1016/jcattod.2015.09.032

[26] S. Rößler, C. Kern, A. Jess, *Chem. Ing. Technol.* **2018**, *90*, 634–642. DOI: https://doi.org/10.1002/cite.201700142

[27] S. Ergun, *Chem. Eng. Prog.* **1952**, *48*, 89–94.

